

The Stochastic Dynamics of an Array of Atomic Force Microscopes in a Viscous Fluid

M. T. Clark* and M. R. Paul

Department of Mechanical Engineering, Virginia Polytechnic and State University, Blacksburg, Virginia 24061

(Dated: February 6, 2008)

We consider the stochastic dynamics of an array of two closely spaced atomic force microscope cantilevers in a viscous fluid for use as a possible biomolecule sensor. The cantilevers are not driven externally, as is common in applications of atomic force microscopy, and we explore the stochastic cantilever dynamics due to the constant buffeting of fluid particles by Brownian motion. The stochastic dynamics of two adjacent cantilevers are correlated due to long range effects of the viscous fluid. Using a recently proposed thermodynamic approach the hydrodynamic correlations are quantified for precise experimental conditions through deterministic numerical simulations. Results are presented for an array of two readily available atomic force microscope cantilevers. It is shown that the force on a cantilever due to the fluid correlations with an adjacent cantilever is more than 3 times smaller than the Brownian force on an individual cantilever. Our results indicate that measurements of the correlations in the displacement of an array of atomic force microscopes can detect piconewton forces with microsecond time resolution.

I. INTRODUCTION

The advent of micro and nanotechnology has ushered forth measurement techniques with unprecedented sensitivity [1, 2, 3, 4]. For example the atomic force microscope (AFM) [5] has revolutionized surface science by enabling topographical measurements with atomic precision [6, 7, 8]. Despite such major advances, a difficult challenge that remains is the measurement of the real time dynamics of single molecules in their natural aqueous environments. For example, the dynamics of proteins such as conformational changes or substrate metabolism occur on force scales of 10's of piconewtons and time scales of 10's of milliseconds [9, 10]. This parameter regime is difficult to reach using current technologies. A promising approach is the use of micro and nanoscale cantilevers [11, 12, 13].

Atomic force microscopy relies upon detecting and interpreting the dynamics of an externally driven micron scale cantilever as it interacts with a sample. The standard approaches of contact, tapping, and non-contact mode involve the active control and driving of the cantilever probe to interact with the sample of interest. The ultimate sensitivity of these measurements is limited by the underlying stochastic thermal motion of the cantilever. An alternative measurement approach is to exploit these stochastic fluctuations. This can be accomplished by placing a passive (or undriven) cantilever in fluid and measuring the resulting stochastic dynamics. The measurement of the thermal noise spectrum is a commonly used calibration technique in atomic force microscopy [14, 15].

Using a passive detection technique, successful measurement then relies upon detecting and interpreting the change in the stochastic dynamics of the cantilever due to the presence or the dynamics of the sample. For ex-

ample, a biomolecule could be tethered between a cantilever and a surface. The stochastic dynamics of the cantilever would then be altered by the dynamics of the linking molecule and its interaction with the fluid as well as the proximity of the surface upon which the molecule is attached. The force sensitivity of this measurement is limited by the Brownian force on the cantilever in the absence of the target biomolecule, i.e. if the dynamics of the attached protein induce forces on the cantilever less than the Brownian force on the cantilever the protein dynamics will be extremely difficult to detect. For a typical atomic force microscope the Brownian force on a single cantilever can be on the order of 100pN (discussed further later) which is too large for many interesting biological measurements [13, 16]. For example, the force measured by Radmacher et al. as the protein lysozyme metabolizes substrate is approximately 50pN [9].

However, such a measurement technique can be significantly improved through the detection of *correlations* in the displacements of the two adjacent cantilevers, for example see Fig. 1(b). The motion of one cantilever will cause fluid motion that will move the adjacent cantilever and vice versa. The Brownian force on each cantilever is uncorrelated and does not contribute to a cross-correlation measurement. The only contribution comes from the correlations due to the fluid which will be significantly reduced in magnitude when compared to the Brownian force felt by a single cantilever. For example, femtonewton forces have been measured from the correlated motion of micron scale spheres held in closely spaced optical traps [17, 18]. Now consider tethering a biomolecule between the two cantilevers in Fig. 1(b). In this case, the motion of the two cantilevers will be correlated by the fluid as well as by the dynamics of the linking target biomolecule. Measurements of the correlations due to the biomolecule could be used to detect the presence of the biomolecule and to probe its biomolecular dynamics in real time.

Prior to the development of such experimental methods the fluidic coupling between adjacent AFM can-

*Electronic address: clarkmt@vt.edu

tilevers must be understood in order to build, design and interpret experiments where the noise from fluid induced correlations is small compared to the forces caused by the dynamics of the tethered biomolecule. The magnitude of the noise induced by fluid correlations in an array of cantilevers is complex and depends upon many factors including cantilever geometry and array configuration. In this paper we explore the fluid induced correlations between two readily available atomic force microscopes in an experimentally motivated opposing configuration. This will provide a baseline understanding of their stochastic dynamics in the absence of a target biomolecule which is essential to the success of future experiments.

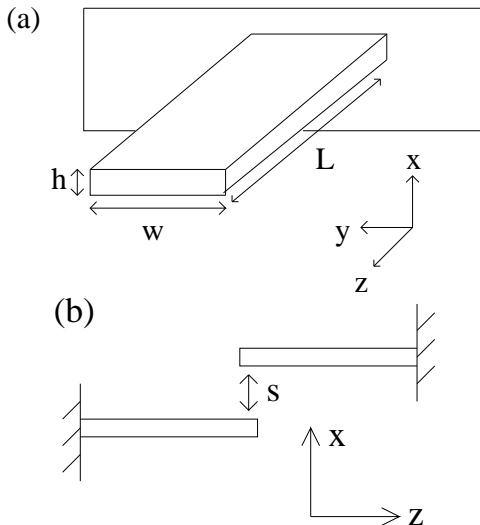


FIG. 1: (a) The convention used in defining the cantilever geometry, not drawn to scale. Actual aspect ratios are $L/h = 98.5$, $w/h = 14.5$, and $L/w = 6.8$. Specific properties of the cantilevers explored here are given in Table I. (b) The configuration of two adjacent AFM cantilevers (not drawn to scale). In the absence of a tethered biomolecule between the cantilevers their motion is correlated due to the induced fluid motion.

Although the cantilever motion is driven by molecular collisions the equations necessary to describe these dynamics are those of classical continuum mechanics. The Knudsen number, Kn , represents the ratio of the mean free path between collisions λ of a fluid molecule to a characteristic length L in the system. In the limit of $\text{Kn} \rightarrow 0$ the continuum hypothesis is valid, however it has been found experimentally to be a good approximation for $\text{Kn} \lesssim 1 \times 10^{-3}$ [19, 20]. For larger values of Kn the continuum hypothesis fails with such consequences as the violation of the no-slip boundary condition at fluid solid interfaces. The relevant length scale L for very long cantilevers is the cantilever half-width $w/2$ from Table I and λ is approximately the diameter of a water molecule, yielding $\text{Kn} = \lambda/L \approx 10^{-5}$. When an array configuration is considered a characteristic length may also be chosen

as the spacing between the cantilevers. For the smallest separation investigated here, $s = 200\text{nm}$, $\text{Kn} \approx 10^{-4}$. Since Kn is small in both situations we will assume that both the continuum and no-slip hypotheses are valid.

To describe the cantilever dynamics the equations of elasticity [21] must be coupled with the equations of fluid dynamics [22]. The fluid coupling of an array of cantilevers is quite complex, and as a result it is useful to discuss the fluid equations in more detail. The Navier-Stokes equations for incompressible fluids are,

$$\beta \frac{\partial \vec{u}}{\partial t} + R \vec{u} \cdot \nabla \vec{u} = -\nabla p + \nabla^2 \vec{u}, \quad (1)$$

$$\nabla \cdot \vec{u} = 0, \quad (2)$$

where $\vec{u} = (u, v, w)$ is the fluid velocity and p is the pressure. The equations are nondimensionalized using the cantilever half-width $w/2$, the maximum cantilever oscillation velocity U , and the inverse cantilever oscillation frequency ω^{-1} as the characteristic length, velocity, and time scales, respectively. On all material boundaries we impose the no-slip fluid boundary condition. The frequency parameter $\beta = w^2 \omega / 4\nu$ is a frequency based Reynolds number and represents the ratio of local inertial forces to viscous forces where ν is the kinematic viscosity of the liquid. The Reynolds number $R = Uw/2\nu$ represents the ratio of convective inertial forces to viscous forces. For the high frequency and low amplitude oscillations of interest here $R \ll 1$ and $\beta \sim 1$ resulting in the unsteady Stokes equations.

An often used approximation for the flow field generated by an oscillating atomic force microscope is that of an infinite cylinder performing transverse oscillations [23]. The fluid dynamics describing the flow field generated can be described in terms of viscous and potential contributions [24]. The potential component reacts instantaneously and depends only upon the position of the cylinder and is out of phase with the cylinder motion. The viscous component is characterized by the diffusion of momentum from the cylinder surface with diffusion constant ν . The phase of the viscous component depends in a complicated manner upon the position of the cylinder. The interplay between the potential and viscous components of the flow field can lead to complex dynamics.

An estimate of the length scale over which viscous effects diffuse during a single cantilever oscillation is given by the Stokes length,

$$\delta_s \approx \left(\frac{\nu}{\omega_f} \right)^{1/2} = \frac{w}{2} \beta^{-1/2}, \quad (3)$$

where ω_f is the resonant frequency for the beam in fluid. For microscale systems this length scale can become quite large, for example a cantilever oscillating at 50 kHz in water yields a Stoke's length on the order of $2 \mu\text{m}$. For very small cantilever separations, as of interest here, the two cantilevers will be immersed in each others Stoke's

layers and their dynamics will be determined by the interactions of the viscous and potential responses. It is important to note that although the fluid dynamics of simple oscillating objects such as cylinders, spheres, and ellipsoids are well known the coupled fluid dynamics of an array of such objects is poorly understood.

The dynamics of a single micron scale cantilever in vacuum can be described using the equipartition theorem for systems in thermal equilibrium [25]. This approach has been extended to include the damping effects of a viscous fluid [23]. In this case, the cantilever was assumed to be long and thin and, as a result, the stochastic dynamics were described by coupling the classical elasticity equations to the flow field caused by an oscillating infinite cylinder. A further simplification in [23] is the assumption that the noise force is frequency independent which is not strictly justified [12, 26].

A recently proposed thermodynamic approach uses the fluctuation-dissipation theorem to predict the stochastic cantilever dynamics through *deterministic* calculations of the coupled fluid-solid equations [12, 26]. Only a brief overview of the method is given here, see Refs. [12, 26] for a detailed discussion. A convenient way to use this approach is to calculate the deterministic dynamics of the cantilevers for the case where one cantilever is exposed to a small step force $f(t)$ given by,

$$f(t) = \begin{cases} F_1 & \text{for } t < 0 \\ 0 & \text{for } t \geq 0. \end{cases} \quad (4)$$

In our simulations the step force is applied to the lower cantilever in Fig. 1(b). Upon removal of the force the lower cantilever returns to equilibrium through underdamped oscillations given by the position of the cantilever tip $X_1(t)$. The fluid motion generated as the lower cantilever returns to equilibrium causes deflections in the tip of the upper cantilever given by $X_2(t)$. The auto and cross-correlations of the equilibrium fluctuations in cantilever displacement are then given by,

$$\langle x_1(0)x_j(t) \rangle = \frac{k_B T}{F_1} X_j(t), \quad (5)$$

where $X_j(t)$ is the deflection of the j^{th} cantilever, k_B is Boltzmann's constant, T is the absolute temperature, and $\langle \rangle$ denotes an equilibrium average in the absence of the step force f . For clarity, a capital $X(t)$ indicates the deterministic cantilever deflection and a small $x(t)$ indicates the stochastic deflection. When $j = 1$ Eq. (5) yields the autocorrelation, and for $j = 2$ it yields the cross correlation. The spectral properties of the correlations are given by the Fourier transform of the auto and cross-correlations to yield the noise spectra, $G_{11}(\omega)$ and $G_{12}(\omega)$.

L	w	h	k	ω_0
197 μm	29 μm	2.0 μm	1.32 N/m	452×10^3 rad/s

TABLE I: Summary of the cantilever geometry and properties. The geometry is given by the cantilever length L , width w , and height h . The cantilever spring constant is k and the resonant frequency in vacuum is ω_0 . The cantilevers are composed of silicon with density $\rho_c = 2320$ kg/m³, and Youngs modulus $E = 1.74 \times 10^{11}$ N/m². The cantilevers are immersed in water with density $\rho_l = 997$ kg/m³ and dynamic viscosity $\eta = 8.59 \times 10^{-4}$ kg/m-s.

m_f/m_e	ω_f/ω_0	Q	β	R
8.2	0.35	3.0	39.0	3.0×10^{-4}

TABLE II: Summary of the cantilever dynamics in fluid as determined from numerical simulations in Ref [26]: the fluid loaded mass of the cantilever m_f , the equivalent cantilever mass m_e , resonant frequency in vacuum ω_0 , resonant frequency in fluid ω_f , the quality Q , the frequency parameter β , and the Reynolds number R . The values of m_f , ω_f , and Q have been determined by fitting the cantilever response to a simple harmonic oscillator.

II. THE STOCHASTIC DYNAMICS OF AN ARRAY OF ATOMIC FORCE MICROSCOPE CANTILEVERS

To explore the stochastic dynamics of two adjacent cantilevers we have performed time-dependent, three dimensional finite element simulations of the governing deterministic fluid-solid equations (algorithm described elsewhere [27, 28]). The AFM cantilevers are micron scale with the simple beam geometry shown in Fig. 1(a). The physical properties of a cantilever are summarized in Table I. The stochastic dynamics of a single cantilever with this geometry in fluid has been explored both experimentally [29] and theoretically [12, 26]. The characteristic quantities to describe its motion are given here in Table II [26]. Most atomic force microscope cantilevers have a probe on the distal end that interacts with the sample of interest [6]. However, in this work we are interested in characterizing the fluid coupling between two stochastic cantilevers and, as a result, we explore the simpler case of two rectangular beams without attached probes. Experimental features such as a probe could be included if desired.

A series of numerical experiments are performed for a range of cantilever separations s , given by $0.1 \leq s/h \leq 2$ where the separation is measured as the distance between the cantilever tips at zero deflection. The minimum cantilever separation investigated here, $s = 200\text{nm}$, is a result of computational constraints given by the numerical method used. The actual cantilever separation in a two-cantilever experiment will depend upon the size

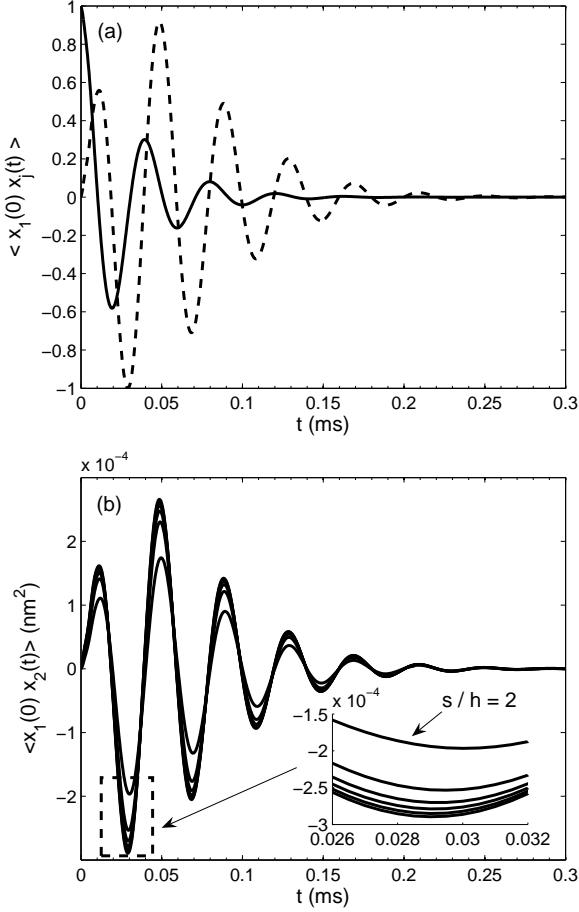


FIG. 2: (a) The autocorrelation (solid line) and cross-correlation (dashed line) of the equilibrium fluctuations in cantilever displacement for $s/h = 0.1$. The two functions have been normalized to highlight the phase difference in the dynamics. The normalization used is $3 \times 10^{-3} \text{ nm}^2$ for the autocorrelation and $2.9 \times 10^{-4} \text{ nm}^2$ for the cross-correlation. (b) Cross-correlation of the equilibrium fluctuations in cantilever displacement over the range of cantilever separations $s/h = 0.1, 0.3, 0.5, 0.7, 1, 2$. (inset) Detailed view of the largest magnitude cross-correlations illustrating a decreasing magnitude with cantilever separation.

and geometry of the cantilever probes [6] and the particular biofunctionalization approach used to tether the biomolecule [13, 30]. Considering readily available cantilever tips and biofunctionalization protocols the range of cantilever separations explored spans what would be expected in experiment [13, 31].

The numerical simulations yield $X_1(t)$ and $X_2(t)$ and the auto and cross-correlations of the equilibrium fluctuations in cantilever displacement are found using Eq. (5). The auto and cross-correlations are shown in Fig. 2 as a function of cantilever separation. The autocorrelation $\langle x_1(0)x_1(t) \rangle$, normalized by its maximum value, is given by the solid line in Fig. 2(a). The autocorrelation did not

depend upon the presence of the adjacent cantilever for all cantilever separations tested and the curve shown is representative for all simulations. The cross-correlation for $s/h = 0.1$, normalized by its maximum value, is also plotted in Fig. 2(a) to clearly illustrate the phase relationship between the auto and cross-correlations. The cross-correlations in the equilibrium fluctuations $\langle x_1(0)x_2(t) \rangle$ are shown in Fig. 2(b). As expected, the magnitude of the cross-correlation decreases as the separation between the two cantilevers is increased (see inset of Fig. 2(b)).

It is useful to look closer at the deterministic flow field caused by an oscillating cantilever that would yield the autocorrelations through Eq. 5. Figure 3 illustrates two different cross-sections of the flow field at $1.5t^*$ where t^* is the time at which the cantilever reaches its maximum velocity. This corresponds to a cantilever tip velocity of $U = 2.5 \text{ mm/s}$ which occurs at a time $t^* = 9.0 \mu\text{s}$, where $t^*/t_p \approx 0.22$ and t_p is the time required for the cantilever to complete its first oscillation. The magnitude of the fluid velocity is less than 1% of the maximum value after a time of $t \approx 20t^*$. The numerical simulation used to generate the flow field of Fig. 3 was for only a single cantilever in fluid to clearly illustrate the three-dimensional nature of the flow field around the tip of an oscillating cantilever. A closer inspection of the flow field reveals that finite fluid velocities extend further in the z -direction than in the y -direction as shown in panels (a) and (b) of Fig. 4, respectively. In other words, the fluid flow over the cantilever tip is greater than the fluid flow around the sides of the cantilever. This suggests that an elastic object located to the side of the cantilever (in the y -direction) will exhibit less fluid coupling than an object placed at the same distance off of the tip of the cantilever (in the z -direction).

Fourier transforms of the cross-correlations yield the noise spectra which are shown in Fig. 5(a) as a function of cantilever separation. It is interesting to note that there is a particular frequency ω^* where the noise spectra vanishes, $G_{12}(\omega^*) = 0$. This knowledge could lead to experimental protocols to minimize the fluid correlated noise. To illustrate this further we plot the behavior of ω^* in Fig. 5(b). The solid line is a linear fit to the data illustrating a steady decrease in ω^* with increasing separation. The reduced frequencies for larger separations are a result of the finite time at which the viscous effects propagate.

Using these results we can characterize the force sensitivity and time resolution of a correlated measurement technique using the cantilever array. An estimate of the force sensitivity can be found using the auto and cross-correlation functions [26],

$$F_{11} = k|\langle x_1(0)x_1(t) \rangle|_{\max}^{1/2}, \quad (6)$$

$$F_{12} = k|\langle x_1(0)x_2(t) \rangle|_{\max}^{1/2}. \quad (7)$$

In our notation, F_{11} represents the magnitude of the stochastic Brownian force acting on a single cantilever. As shown by the solid line in Fig. 2(a) the maximum

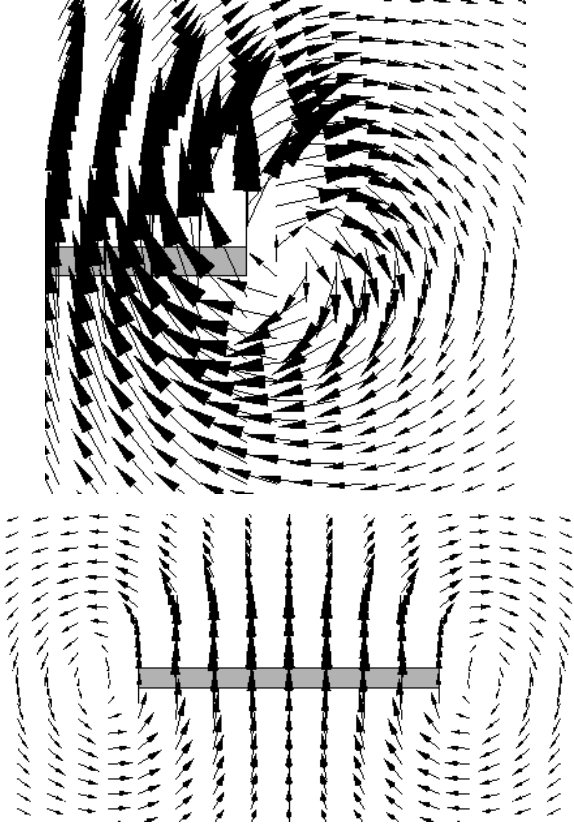


FIG. 3: The three-dimensional flow field near the tip (distal end) of an oscillating atomic force microscope. The flow field is a snap shot in time at the instant where the cantilever is at its maximum velocity, $t^* = 9.0\mu\text{s}$. (top) Flow field over the cantilever tip in the $x - z$ plane. The base of the cantilever is to the far left of the figure and is not shown. (bottom) Flow field around the sides of the cantilever in the $x - y$ plane. See Fig. 1 for coordinate axis definitions. In both figures the largest arrow indicates a fluid velocity of $U = 2.5$ mm/s.

value of the autocorrelation occurs at time $t = 0$ which is the root-mean-squared deflection of the stochastic motion. Using the equipartition theorem, this is given by the simple expression [32],

$$\langle x^2 \rangle^{1/2} = \sqrt{\frac{k_B T}{k}}, \quad (8)$$

which yields 0.56\AA . The magnitude of the thermally driven oscillations are much smaller than the thickness of the cantilever, $\langle x^2 \rangle^{1/2}/h = 2.8 \times 10^{-5}$. In this case, the Brownian force on an individual cantilever is $F_{11} = (k_B T k)^{1/2} = 74\text{pN}$.

In a cross-correlation measurement between two cantilevers the Brownian noise felt by the two individual cantilevers is uncorrelated and does not contribute. This leaves only the correlations due to the fluidic induced correlations. F_{12} represents the approximate magnitude of the force due to these hydrodynamic correla-

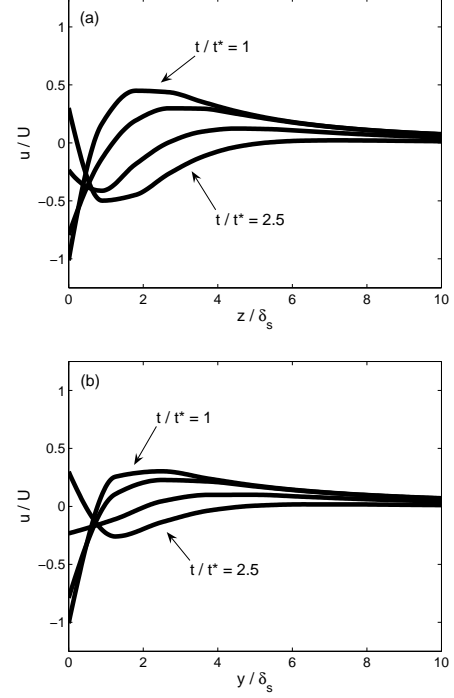


FIG. 4: (a) The variation in the x-component of the fluid velocity u as a function of distance in the z -direction measured from the tip of the cantilever at various times during the cantilevers oscillations. (b) The variation in the x-component of the fluid velocity u as a function of distance in the y -direction measured from the tip of the cantilever at various times during the cantilevers oscillations. In each plot curves are shown for $t/t^* = 1, 1.5, 2, 2.5$, where $t/t^* = 1$ and 2.5 are labeled and the other two are in sequence.

tions. From Fig. 2(b) for the case with the closest separation, $s/h = 0.1$, the maximum magnitude of the cross-correlation $|\langle x_1(0)x_2(t) \rangle|_{max} \approx 2.9 \times 10^{-4}\text{nm}^2$ which yields a root-mean-squared displacement of 0.17\AA . Using Eq. (7) this yields a force sensitivity of approximately 22 pN, an improvement of better than three fold over the force noise acting on a single cantilever. The variation in F_{12} with cantilever separation is shown in Fig. 6. The force due to fluid correlations decreases with separation and the solid line represents a quadratic polynomial curve fit to the data. The reduction in the noise is quite gradual over the separations of interest. The noise reduction at the largest separation $s = 2\mu\text{m}$ is a 4-fold improvement over a single cantilever.

An estimate of the time resolution possible is given by the time it takes the cantilever to complete an oscillation at its resonant frequency. Using the parameters obtained from the simple harmonic oscillator curve fit for a single cantilever in fluid, this time scale is estimated to be $\tau \approx 2\pi/\omega_f = 39\mu\text{s}$ which yields a measurement frequency of 25 kHz. Therefore the cantilever array investigated here can measure forces on the order of 10^5

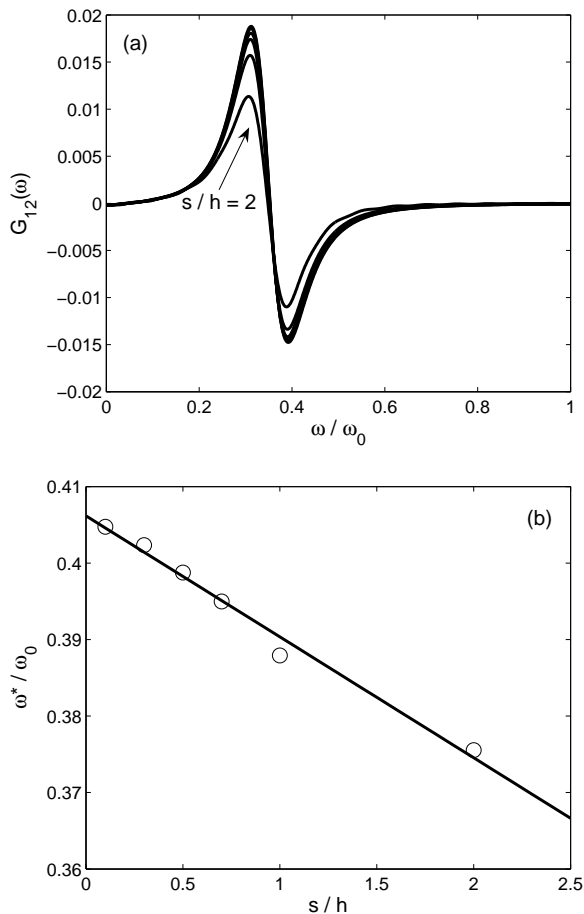


FIG. 5: (a) The noise spectrum $G_{12}(\omega)$ for the cantilever array, normalized by the same factor as $G_{11}(\omega)$ in [26]. Results are shown for cantilever separations of $s/h = 0.1, 0.3, 0.5, 0.7, 1, 2$. The curve for $s/h = 2$ is labelled and the others are in sequential order. (b) The frequency at which the spectral response crosses zero ω^* as a function of separation. The solid line is a linear curve fit given by $\omega^*/\omega_0 = -1.58 \times 10^{-2}(s/h) + 0.406$.

of pN with kHz frequency resolution which would make possible the real time measurements of many interesting molecular interactions [9, 16].

As mentioned, the length over which viscous effects act can be quite large for microscale systems. To ensure that the simulation boundaries do not significantly affect the results a series of numerical tests were performed using varying numerical domain sizes. The size of the numerical domain to be used for analysis was chosen such that the magnitude of the fluid velocity went gradually to zero at the walls. Specifically, the distance between the cantilever tip and any numerical bounding wall is chosen such that the velocity field at $t/t^* = 1$ gradually decreases to a value less than 1% of the maximum velocity before reaching a solid wall. Numerical results indicate that the distance from the cantilever tip

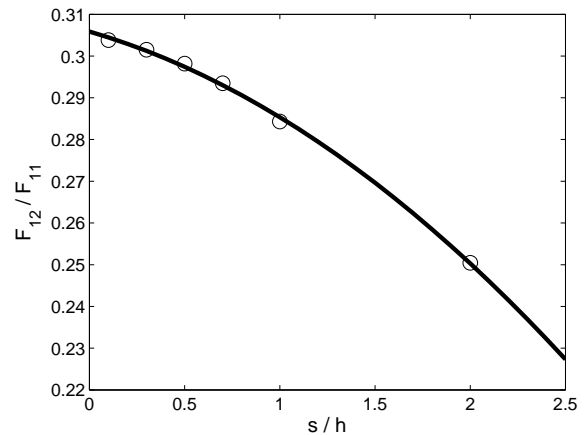


FIG. 6: Force sensitivity F_{12} as a function of AFM cantilever separation. Forces have been normalized by the Brownian force on a single cantilever ($F_{11} = 74$ pN). The solid line is a quadratic curve fit to the data and is given by $F_{12}/F_{11} = -7.3 \times 10^{-3}(s/h)^2 - 1.33 \times 10^{-2}(s/h) + 0.306$.

to the walls should be at least $24\delta_s$ in both y and z , and $12\delta_s$ in x . The numerical domain was chosen to be larger than these constraints in each direction for all numerical simulations presented here. Results from simulations where the numerical domain was smaller than these values yielded cantilever dynamics with lower values of Q and ω_f in agreement with the predicted increase in dissipation for a cantilever oscillating near a wall [33, 34].

III. CONCLUSIONS

The correlated stochastic dynamics of an array of two AFM cantilevers have been obtained using a thermodynamic approach with deterministic numerical calculations. Measurements of the correlations in cantilever displacement yield force sensitivities that are improved by a factor of 3 to 4 over the range of interest for cantilever separations that may be useful for single molecule experiments. The complex flow field around the tip of an oscillating cantilever suggests that the configuration of the cantilever array is an important determining factor in the resulting cantilever correlations. The approach used here is quite general and can be extended to include more complex geometries and array configurations that are motivated by experiment. Theoretical calculations, such as these, will provide important insight necessary for the interpretation and design of future micro and nanoscale technologies that exploit inherent thermal fluctuations.

IV. ACKNOWLEDGMENTS

This research has been partially supported by DARPA/MTO Simbiosys under grant F49620-02-1-0085

and an ASPIRES grant from Virginia Tech. We gratefully acknowledge extensive interactions with S. Quake, M.C. Cross, and the Caltech BioNEMS effort (M.L. Roukes, PI).

-
- [1] C. Bustamante, J. Macosko, and G. Wuite, *Nature Reviews* **1**, 130 (2000).
 - [2] M. L. Roukes, *Nanoelectromechanical systems*, cond-mat/0008187 (2000).
 - [3] H. Craighead, *Science* **290**, 1532 (2000).
 - [4] J. L. Arlett, J. R. Maloney, B. Gudlewski, M. Muluneh, and M. L. Roukes, *Nano Lett.* **6**, 1000 (2006).
 - [5] G. Binnig, C. F. Quate, and C. Gerber, *Phys. Rev. Lett.* **56**, 930 (1986).
 - [6] R. Garcia and R. Perez, *Surface Science Reports* pp. 197–301 (2002).
 - [7] F. J. Giessibl, *Reviews of modern physics* **75**, 949 (2003).
 - [8] P. K. Hansma, J. P. Cleveland, M. Radmacher, D. A. Walters, P. E. Hillner, M. Benzanilla, M. Fritz, D. Vie, H. G. Hansma, C. B. Prater, et al., *Appl. Phys. Lett.* **64**, 1738 (1994).
 - [9] M. Radmacher, M. Fritz, H. Hansma, and P. K. Hansma, *Science* **265**, 1577 (1994).
 - [10] N. H. Thomson, M. Fritz, M. Radmacher, J. Cleveland, C. F. Schmidt, and P. K. Hansma, *Biophys. J.* **70**, 2421 (1996).
 - [11] M. B. Viani, T. E. S. Schaffer, and A. Chand, *Journal of Applied Physics* **86**(5), 2258 (1999).
 - [12] M. R. Paul and M. C. Cross, *Physical Review Letters* **92**(23), 235501 (2004).
 - [13] J. L. Arlett, M. R. Paul, J. Solomon, M. C. Cross, S. E. Fraser, and M. L. Roukes, in *Controlled Nanoscale Motion in Biological and Artificial Systems* (Springer-Verlag, 2005), Nobel Symposium 131.
 - [14] Y. Martin, C. C. Williams, and H. K. Wickramasinghe, *J. Appl. Phys.* **61**, 4723 (1987).
 - [15] J. Cleveland, S. Manne, D. Bocek, and H. P.K., *Rev. Sci. Instrum.* **64**, 403 (1993).
 - [16] G. Bao and S. Suresh, *Nature Materials* **2**, 715 (2003).
 - [17] J. C. Meiners and S. R. Quake, *Physical Review Letters* **82**(10), 2211 (1998).
 - [18] J. C. Meiners and S. R. Quake, *Physical Review Letters* **84**(21), 5014 (2000).
 - [19] S. A. Schaaf and P. L. Chambre, *Flow of rarefied gases* (Princeton University Press, 1961).
 - [20] G. Karniadakis, A. Beskok, and N. Aluru, *Micro flows* (Springer, 2001).
 - [21] L. D. Landau and E. M. Lifshitz, *Theory of elasticity* (Butterworth-Heinemann, 1959).
 - [22] R. L. Panton, *Incompressible fluid flow* (Wiley, 2005).
 - [23] J. E. Sader, *J. Appl. Phys.* **84**, 64 (1998).
 - [24] L. Rosenhead, *Laminar Boundary Layers* (Oxford University Press, 1963).
 - [25] H.-J. Butt and M. Jaschke, *Nanotech.* **6**, 1 (1995).
 - [26] M. R. Paul, M. Clark, and M. C. Cross, *Nanotechnology*, to be published (2006).
 - [27] CFD Research Corporation, 215 Wynn Dr. Huntsville AL 35805.
 - [28] H. Q. Yang and V. B. Makhijani, *AIAA-94-0179* pp. 1–10 (1994).
 - [29] J. W. M. Chon, M. P., and J. E. Sader, *Journal of Applied Physics* **87**(8), 3978 (2000).
 - [30] J. Solomon and M. Paul, *Biophys J.* **90**, 1842 (2006).
 - [31] NanoScience Instruments, store.nanoscience.com.
 - [32] T. R. Albrecht and C. F. Quate, *J. Appl. Phys.* **62**, 2599 (1987).
 - [33] C. P. Green and J. E. Sader, *Phys. Fluids* **17**, 073102 (2005).
 - [34] R. J. Clarke, S. M. Cox, P. M. Williams, and O. E. Jensen, *J. Fluid Mech.* **545**, 397 (2005).